In vivo NMR detection of diet-induced changes in adipose tissue composition

Rosa T. Branca[1] **and Warren S. Warren**

Chemistry Department, Duke University, Durham, NC

Abstract We introduce an in vivo spectroscopic method to assess the effects of diet on fatty acid composition of the predominant chemical constituent of adipocytes in mice. To do this, we make use of a nonlinear NMR signal that, unlike a standard NMR signal, is intrinsically insensitive to local magnetic field inhomogeneities and which naturally suppresses the large water signal from nonfatty tissues. Our method yields fat composition information from fat depots distributed over large sample volumes in a single experiment, without requiring the use of tedious shimming procedures, voxel selection, or water suppression. Our results suggest that this method can reveal clear differences in adipose tissue composition of mice fed a standard chow diet compared with mice fed a diet rich in polyunsaturated fatty acids. With further developments this method could be used to obtain information on human lipid composition noninvasively and to track changes in lipid composition induced by diet intervention, pharmaceutical drugs, and exercise.—Branca, R. T., and W. S. Warren. **In vivo NMR detection of diet-induced changes in adipose tissue composition. *J. Lipid Res.* 2011.** 52: **833–839.**

Supplementary key words NMR spectroscopy • saturated fatty acids • unsaturated fatty acids • intermolecular zero quantum coherences

In both preclinical and clinical metabolic research, a method for in vivo detection of tissue fatty acid composition would be invaluable. Fatty acids are known to affect cellular metabolism through the control of signal-transduction pathways (1) and gene expression (2, 3), and alteration in their profile is often indicative of human diseases such as diabetes (4), inflammation (5), or cancer (6, 7). As fatty acid composition can also be affected by dietary fat, dietary fats are assumed to have an important role on extracellular and intracellular lipid metabolism. Several studies have demonstrated that diets rich in saturated fatty acids increase intracellular lipid accumulation and cause insulin resistance (8), while diets rich in fish oil are shown to protect against fat-induced insulin resistance (9, 10).

Despite its importance, tissue fatty acid composition is difficult to study in vivo. NMR can be used to detect saturation and unsaturation level of fatty acids. Because of the difference in chemical shift between the different protons in the lipid molecule, one can easily and noninvasively determine the ratio between saturated and unsaturated fatty acids using ^{13}C (11-13) and ^{1}H NMR (14). Although ^{1}H NMR offers higher sensitivity than ^{13}C, this analysis is difficult to accomplish in vivo, where magnetic susceptibility gradients caused by interfaces between the target tissue and air, bone, or capillary vessels dramatically broaden resonance frequency lines and degrade spectral resolution.

To improve spectral resolution, the NMR signal is usually acquired from very small voxels after careful shimming procedures and MRI-guided voxel localization (15–17). In the liver, this method has proven to be very useful to differentiate benign hepatic steatosis from the more progressive forms of fatty liver. Specifically, the degree of unsaturation of hepatic lipid, which is associated with an elevated omega-6/omega-3 fatty acid ratio, has been correlated with increased oxidative stress that occurs in steatohepatitis and type 2 diabetes mellitus patients (18, 19). For hepatocellular carcinoma, one of the most deadly forms of cancer, in vivo NMR lipid profiling has demonstrated early diagnoses. Alterations in the unsaturation level of hepatic lipids, and therefore in lipid metabolism, can indeed be detected well before the neoplastic nodules become visible in MRI scans (20). It has also been demonstrated that this method can be a very important tool for differentiating quiescent atherosclerotic plaques from more active plaques that lead to acute ischemic syndromes. Because of its ability to detect cholesteryl ester, a lipid spe-

This work was supported by National Institutes of Health Grants R21 DK-090758 and by R01 EB-002122. Its contents are solely the responsibility of the authors and do not necessarily represent the official views of the National Institutes of Health.

Manuscript received 26 October 2010 and in revised form 24 January 2011.

Published, JLR Papers in Press, January 26, 2011
DOI 10.1194/jlr.D012468

Abbreviations: 1D, one dimension; 2D, two dimension; HOMOGENIZED, homogeneity enhancement by intermolecular zero quantum detection; iDQC, intermolecular double-quantum coherence; iSQC, intermolecular single-quantum coherence; iZQC, intermolecular zero-quantum coherence; PRESS, point-resolved spectroscopy; WAT, white adipose tissue.

[1]To whom correspondence should be addressed.
e-mail: tamara.branca@duke.edu

cifically linked to plaque rupture, NMR spectroscopy seems very well suited for identifying vulnerable plaque noninvasively prior to the occurrence of an atherothrombotic event (21). The shimming procedure associated with this method, however, is time consuming, and the method itself requires careful localization to exclude tissue interfaces and areas with strong susceptibility gradients. Moreover, the method suffers from chemical shift displacement artifacts that rise sharply with reduced voxel size. This precludes the possibility to use such a technique to analyze large body areas or tissues that are highly heterogeneous.

We present here a new approach to analyze the fatty acid composition of fat depots spread over large (several cubic centimeter) volumes, without loss of spectral resolution and without signal contamination from lean tissues. This approach is based on the detection of the nonlinear signal from intermolecular zero quantum coherences (iZQC), which is well known to be insensitive to magnetic field inhomogeneities and which has previously been used to enhance spectral resolution in a deshimmed sample (22), for a strongly drifting magnet (23), and in vivo (24–26). The iZQC signal is sensitive to simultaneous opposing transitions of two or more spins on different molecules. These transitions are not directly observable like a standard linear NMR signal, and their detection requires the acquisition of a bi-dimensional (2D) spectrum. This 2D spectrum is acquired with a pulse sequence that has been modified from the standard homogeneity enhancement by intermolecular zero quantum detection (HOMOGENIZED) iZQC pulse sequence (22) to specifically detect the iZQC signal between the methylene spins at 1.3 ppm and all other nearby proton spins in a 100 μm range. Water signal from lean tissues, which lack nearby (<100 μm) methylene spins, is thereby naturally suppressed. Extra water suppression modules are therefore unnecessary, and the presence of lean tissue in the selected volume does not affect spectral quality. Moreover, since the signal is naturally insensitive to magnetic field inhomogeneities, the technique can be used to analyze large volumes. Signal from physiologically distributed lipid depots contributes to overall signal without compromising spectral resolution.

We have calibrated and validated this method for samples containing known amounts of fatty acids, and then used it in vivo on mice to measure adipose tissue composition changes induced through dietary intervention.

MATERIAL AND METHODS

In vivo studies

All animal studies were approved by the Duke University Institutional Animal Care and Use Committee. They were performed using 8-week-old C57 male mice from the same litter (n = 4) and a 24-month-old obese (ob/ob) mouse (n = 1). All animals were housed at a constant temperature (20-24°C) in 12-h light/dark cycles. Mice were divided in two groups (two mice per group) and fed ad libitum with either a standard chow diet (11% kcal from fat) or with standard chow diet supplemented with flaxseed oil, (flaxseed oil softgel, SPECTRUM, Boulder, CO), rich in polyunsaturated fatty acids (PUFA).

The MR experiments were performed at 4 weeks and at 12 weeks during the diet regimen. In preparation for the MR experiments, all animals were fed 32 h prior to the imaging experiments with standard chow. For the experiments, animals were induced with Nembutal (60 mg/kg) in a single intra-peritoneal injection before the study. During the imaging study, anesthesia was maintained with periodic injection of Nembutal at 1/4 the initial dose, and the free-breathing animals were monitored using MR-compatible animal monitoring equipment from SA Instruments (Stony Brook, NY). Body temperature was monitored with a rectal temperature probe and regulated and maintained using forced heated air. A total of three spectra, acquired every 30-50 min, were acquired for each animal and for each time point.

NMR spectroscopy studies

All MR experiments were performed on a 7T small animal magnetic resonance tomograph with a 210 mm inner bore diameter, interfaced to a Bruker Biospec console (Bruker BioSpin MRI GmbH, Ettlingen, Germany). The system was equipped with a gradient coil system (maximum gradient strength 42 Gauss/cm) and a ^{1}H transmitter-receive coil with a 35 mm inner diameter.

Coronal respiratory-gated spin echo images (Fig. 2A and Fig. 3A, B) were first acquired for morphological reference with the following parameters: an echo time (TE) of 14 ms, a repetition time (TR) of 3 s, a matrix size of 256 × 128, a field of view (FOV) of 6 cm × 3 cm, and a slice thickness of 2 mm.

For the nonlocalized ^{1}H spectrum, we used a 90° broadband pulse (1 ms Hermite pulse) followed by an acquisition window of 500 ms. For the localized ^{1}H spectra, we used a point-resolved spectroscopy (PRESS) sequence, with TR = 4 s, TE = 9.5 ms, and 400-800 averages, without solvent suppression. For these spectra, we selected voxel sizes ranging from 1 × 1 × 1 mm^3 to 2 × 2 × 2 mm^3 located in the abdominal fat depot of the mouse.

The 2D iZQC spectra were all acquired with the sequence shown in **Fig. 1**, which was customized to selectively detect methylene protons (-CH_2-) at 1.3 ppm that are spatially coupled with all the other lipid protons: the olefinic methylene protons (-CH = CH-) at 5.3 ppm, the allylic protons at 2.03 ppm, the α methylene protons at 2.25 ppm, and the bisallylic protons at 2.77 ppm. Water spins from lean tissue, and uncoupled water and fat spins are dephased by a combination of gradient pulses, selective RF excitations, and RF phase cycling. In the sequence, the first 90° pulse (Hermite, 1ms duration) excited all orders of coherences, including zero-quantum (iZQC) and double-quantum (iDQC) coherences. The frequency selective 180° pulse (Gaussian, 3.425 ms) applied at 1.3 ppm cross-converted mixed spin iDQC with iZQC. A final 90° broadband pulse (Hermite, 1 ms) at 4.7 ppm converted iZQC and iDQC coherences to detectable single-quantum (iSQC) antiphase magnetization. The sequence did not have a volume selective module but, after the mixing pulse, a slice selective refocusing pulse (Hermite, 1ms), surrounded by crusher gradients, was applied to selectively refocus the signal from a 40 mm slice centered in the lower abdomen. In our case, the iDQC→iZQC→iSQC coherence transfer pathway was selected by a gradient combination of G1:G2:G3 = 8:-14:16 Gauss/cm, with a 1ms duration. A crusher module (90° RF pulse surrounded by pulsed field gradients of different strengths oriented along the magic angle) at the beginning of the sequence dephased any signal from stimulated echoes. For the acquisition of the 2D spectra, the tau delay (tau = 3.7 ms) was kept constant, while the t1 delay (t1 = 3.4595 ms), during which the iZQC signal evolves, was stepped 128 times in increments of 0.333 ms, resulting in a spectral bandwidth of 3,000 Hz along the indirectly detected spectral dimension (F1). The signal for each t1 point was then collected with a repetition time (TR) of 3 s, an echo time (TE) of 29 ms, a

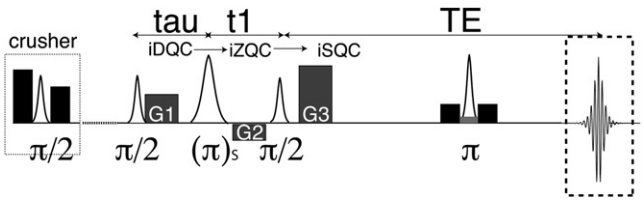

Fig. 1. iZQC pulse sequence used to collect 2D spectra from the abdomen of the different animals. The sequence begins with a crusher module [consisting of a 90 degree broadband pulse surrounded by two pulsed field gradients of different intensities (black boxes)]. After the crusher module and a delay time of about 2.8 s (dotted line), the first broadband ($\pi/2$) excitation pulse is applied. This pulse excites all coherences, including iDQCs. The iDQCs evolve for a constant time delay (tau) and are then transformed into iZQCs by a selective inversion pulse [$(\pi)_s$] acting on the methylene spins. The iZQCs then evolve for a variable time (t1), after which they are transformed by a broadband ($\pi/2$) degree pulse to standard SQCs. The signal is then acquired after a time (TE) after the third mixing pulse. During TE, a slice-selective (π) pulse, surrounded by crusher pulsed field gradients (black boxes), is used to refocus the signal. The G1, G2, and G3 gradients are the pulse field gradients used to select the coherence pathway indicated in the figure (iDQC→iZQC→iSQC). 2D, two dimension; iDQC, intermolecular double-quantum coherence; iZQC, intermolecular zero-quantum coherence; SQC, single-quantum coherence.

number of repetitions (NEX) of 4, a bandwidth of 3000 Hz, and 128 complex data points.

Post-processing was then performed using Matlab software. Data processing consisted of a DC offset removal and a complex 2D Fourier transformation. The 2D spectra, each with 128 × 128 spectral points, were then linearly interpolated to give 512 × 512 spectral points. In the resulting 2D spectrum, the peak position in the F1 dimension was given by the resonance frequency difference between the participating spins; it is insensitive to resonance frequency offsets. For example, the resonance frequency of the (F1 = P2-P4, F2 = P4) iZQC peak along the indirectly detected dimension F1 is $\omega_{P2-P4} = \omega_{P2} - \omega_{P4} = (1.3 - 2.03)ppm = 0.73ppm = 220Hz$ at 7T, while the resonance frequencies of the P5-P2 and P6-P2 peaks were at 285 Hz and 441 Hz, respectively, at 7T.

The volume integral is then measured for the three cross-peaks (P4-P2, P5-P2, P6-P2), and then the ratios, $volume\left(\frac{ZQC_{(P6-P2)}}{ZQC_{(P5-P2)}}\right)$ and $volume\left(\frac{ZQC_{(P4-P2)}}{ZQC_{(P5-P2)}}\right)$, were calculated to determine the adipose tissue unsaturation and polyunsaturation level, as described below.

All iZQC experiments were performed under free breathing without respiratory gating.

Calculation of triglyceride composition

For standard 1D spectroscopy, the unsaturation and polyunsaturation level of lipid depots could be determined by measuring the area under the three peaks that span the 2-2.8 ppm range of the standard ^{1}H spectrum: the allylic peak (P4) at 2.03 ppm, the α methylene peak (P5) at 2.25 ppm, and the bisallylic peak (P6) at 2.77 ppm (15, 16). More specifically, the ratio between the allylic protons (P4) and the α methylene protons (P5) could be used to measure the fraction of fatty acids that are unsaturated (F_{unsat}),

$$F_{unsat} = \frac{1}{2} area\left(\frac{P4}{P5}\right),$$

while the ratio between the bisallylic protons (P6) and the α methylene protons (P5) yielded information on the fraction of fatty acids that are polyunsaturated [disaturated (F_{disat}) or triunsaturated ($F_{triunsat}$)]. Assuming that higher unsaturated fatty acids in the fat depots of humans or mice are scarce, we could write:

$$F_{disat} + 2 * F_{triunsat} = area\left(\frac{P6}{P5}\right).$$

In the iZQC spectrum, unlike in the standard 1D spectrum, each peak represented a coupling between two different spins. The P4-P2 peak, for example, represented the coupling between the allylic spins and the bulk methylene spins, while the P5-P2 peak represented the coupling between the α methylene spins and the bulk methylene spins (Fig. 1C). The intensity of these peaks is, to a first approximation, proportional to the concentration of the two correlated spins:

$$M_{iZQC(P4-P2)} \propto M_{0,P2} M_{0,P4} TE$$
$$M_{iZQC(P5-P2)} \propto M_{0,P2} M_{0,P5} TE$$
$$M_{iZQC(P6-P2)} \propto M_{0,P2} M_{0,P6} TE$$

Therefore, when we considered the ratio between any two of these peaks, we could ignore the methylene contribution to the signal and assume that, as in standard 1D ^{1}H spectroscopy:

$$F_{unsat} = \frac{1}{2} volume\left(\frac{ZQC_{(P4-P2)}}{ZQC_{(P5-P2)}}\right)$$
$$F_{disat} + 2 * F_{triunsat} = volume\left(\frac{ZQC_{(P6-P2)}}{ZQC_{(P5-P2)}}\right)$$

Once these ratios were measured, correction factors needed to be used to compensate for relaxation, which can have a strong effect because the delay before the first excitation pulse and signal acquisition is usually on the order of tens of milliseconds. To account for relaxation, we needed to correct the measured value by a factor of $e^{\left(-TE_{tot}/T_{2,P5}+TE_{tot}/T_{2,P4}\right)}$ for the $volume\left(\frac{ZQC_{(P4-P2)}}{ZQC_{(P5-P2)}}\right)$ ratio, and $e^{\left(-TE_{tot}/T_{2,P5}+TE_{tot}/T_{2,P6}\right)}$) for the $volume\left(\frac{ZQC_{(P6-P2)}}{ZQC_{(P5-P2)}}\right)$ ratio. If we assume the values found by Strobel et al. (16) for the transverse relaxation times of the P4, P5, and P6 peaks, we could estimate a correction factor of 1.38 for the $volume\left(\frac{ZQC_{(P4-P2)}}{ZQC_{(P5-P2)}}\right)$ ratio, and of 0.7 for the $volume\left(\frac{ZQC_{(P6-P2)}}{ZQC_{(P5-P2)}}\right)$ ratio (as TE_{tot} we assume dTE + tau + t1 = 36 ms).

By considering transverse relaxation effects on the three different peaks, we could then rewrite:

$$F_{unsat} = \frac{1}{2} volume\left(\frac{ZQC_{(P4-P2)}}{ZQC_{(P5-P2)}}\right) \cdot e^{\left(-TE_{tot}/T_{2,P5}+TE_{tot}/T_{2,P4}\right)}$$
$$F_{disat} + 2 * F_{triunsat} = volume\left(\frac{ZQC_{(P6-P2)}}{ZQC_{(P5-P2)}}\right) \cdot e^{\left(-TE_{tot}/T_{2,P6}+TE_{tot}/T_{2,P4}\right)} \quad \textit{(Eq. 1)}$$

Experimental estimation of calibration factors

Correction factors could also be found experimentally by measuring the $volume\left(\frac{ZQC_{(P4-P2)}}{ZQC_{(P5-P2)}}\right)$ and the $volume\left(\frac{ZQC_{(P6-P2)}}{ZQC_{(P5-P2)}}\right)$ ratios for a sample with known amounts of saturated and unsaturated

fatty acids. For this study, we used pure (>99%) oleic and linoleic acids, obtained from Sigma-Aldrich (St. Louis, MO), which have 18 carbon chains and one and two double-bonded sites, respectively. IZQC experiments were run on these samples, and all measurements were repeated three times with slightly different shim settings. We then found the experimental calibration factors by measuring the peak volume integral ratio of the three nonoverlapping signals from the iZQC spectrum (P4-P2, P5-P2, P6-P2) and by comparing them with the expected theoretical value in absence of relaxation. From the difference between the expected theoretical ratio and the experimental ratio, we obtained a correction factor of 1.3 ± 0.1 for the (P4-P2)/(P5-P2) ratio and a correction factor of 0.45 ± 0.08 for the (P6-P2)/(P5-P2) ratio.

RESULTS

Good agreement was found between the experimental (1.3 ± 0.1) and theoretically derived (1.38) correction factors for $volume\left(\frac{ZQC_{(P4-P2)}}{ZQC_{(P5-P2)}}\right)$. On the other hand, the correction factor found experimentally (0.45 ± 0.08) for $volume\left(\frac{ZQC_{(P6-P2)}}{ZQC_{(P5-P2)}}\right)$ was quite different from what we predicted theoretically (0.7). This is because we did not consider the effect that the selective narrowband RF pulse, used in the sequence to interconvert iDQC into iZQC, had on the different spins. Unlike the other broadband pulses (1 ms Hermite pulse with a 5400 Hz bandwidth), this selective pulse (3.425 ms Gaussian pulse with a 800 Hz bandwidth), centered on the methylene spins at 1.3 ppm, enhanced the iZQC coupling that the methylene spins have with the bisallylic spins and attenuated the iZQC coupling that the methylene spins have with the α methylene spins, resulting in further enhancement of the $volume\left(\frac{ZQC_{(P6-P2)}}{ZQC_{(P5-P2)}}\right)$ ratio.

We estimated this effect by measuring the methylene signal attenuation as a function of the resonance frequency offset of this pulse. This enhancement is about 1.55, and it brings the expected correction factor from 0.7 to 0.7/1.55 = ~0.45, which is similar to what we found experimentally (0.45 ± 0.08).

Figure 2 shows the anatomical image along with the corresponding 1D NMR spectrum and the 2D iZQC spectrum obtained from the obese mouse. A comparison of the iZQC spectrum with the standard 1D spectrum acquired from the same region shows impressive resolution enhancement and excellent water suppression. In addition to coupling of the CH_2 methylene protons with the CH_3 protons (P2-P1) and CH_2 (P2-P2), coupling with the olefinic (P2-P9), allylic methylene (P2-P4), alpha methylene (P2-P5), and diallylic methylene (P2-P6) peaks are easily identified and resolved. This confirms the theoretical prediction that iZQC is insensitive to magnetic field inhomogeneities and that water signal from lean tissue is naturally suppressed.

Figure 3 shows a representative expansion of the (P4-P2)/(P6-P2) spectral peak region generated from the two groups of mice at 4 and 12 weeks. The signals from all couplings are well separated, thus permitting their straightforward integration for calculating fatty acid composition. Changes in fatty acid composition due to PUFA diet are clearly observed in the iZQC spectra and confirmed by standard localized PRESS experiments (Fig. 3G, H). The P6-P2 peak, corresponding to PUFAs, is highly enhanced in the PUFA diet group and increases over time with respect

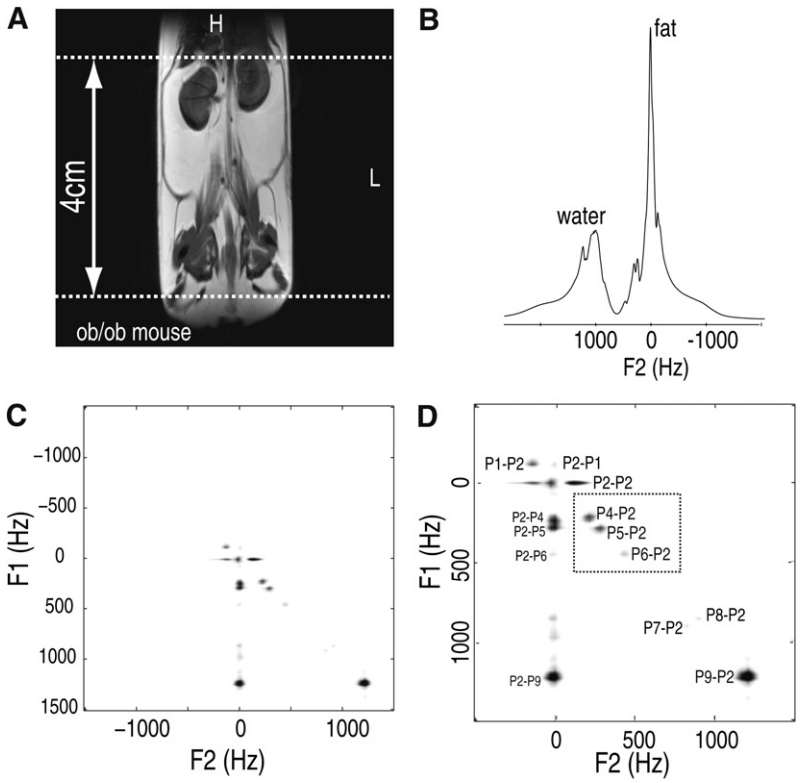

Fig. 2. A: Coronal MRI slice through the abdominal region of an obese mouse showing (white dotted lines) the selected abdominal slice analyzed with our method. The positioning of the mouse is indicated by the letters H (head) and L (left). B: Standard 1D spectrum acquired from the same mouse. For the acquisition of this spectrum, we used a 90° excitation pulse with a TR = 3.5 s and NA = 1. C-D: Representative in vivo iZQC proton spectrum of the selected area of the obese mouse. Shown are eight different iZQC lipid-lipid peaks: (P1-P2), methylene-methylene IZQC (P2-P2), allylic-methylene (P4-P2), α methylene-methylene (P5-P2), bis-allylic-methylene (P6-P2), glycerol-methylene (P7-P2 and P8-P2), and olefinic-methylene (P9-P2). 1D, one dimension; iDQC; intermolecular double-quantum coherence; iZQC, intermolecular zero-quantum coherence.

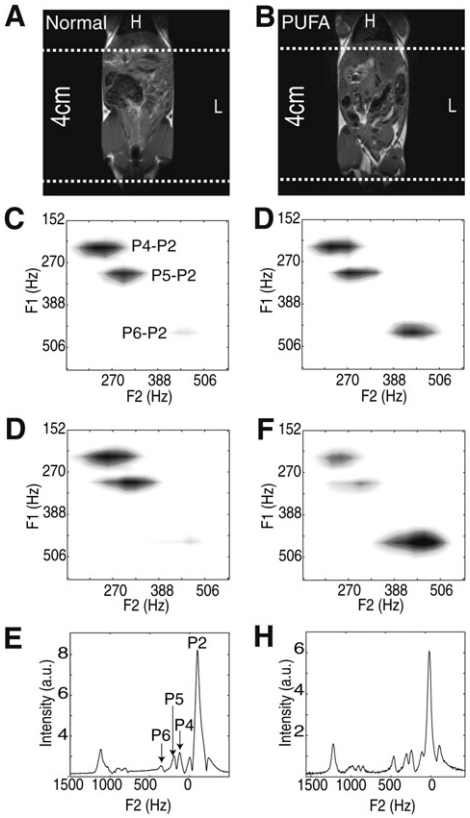

Fig. 3. A-B: Coronal MRI spin-echo images showing the selected slice of a mouse fed standard chow (A) and a mouse whose diet is supplemented with PUFA (B). C-D: iZQC spectra from the two groups after 4 weeks, showing the region highlighted in Fig 2D. Spectrum from a mouse fed standard chow (C), and spectrum from a mouse whose diet is supplemented with PUFA (D). E-F: iZQC spectra from the two groups after 12 weeks, showing the region highlighted in Fig. 2D. Spectrum from a mouse eating standard chow (E), and spectrum from a mouse whose diet is supplemented with PUFA (F). G-H: Localized ^{1}H spectra from the two groups after 12 weeks. Localized ^{1}H PRESS spectrum from a $2 \times 2 \times 2$ mm^3 voxel centered in the intra-abdominal fat depot of a mouse fed standard chow (G), and localized ^{1}H PRESS spectrum from a $1 \times 1 \times 1$ mm^3 voxel centered in the intra-abdominal fat depot of a mouse fed standard chow and PUFA supplements (F). iZQC, intermolecular zero-quantum coherence spectroscopy.

to the P4-P2 peak, reflecting the change in lipid composition that occurs over time under the PUFA diet. The relative ratios of saturated versus unsaturated fatty acids, calculated by using the experimental calibration factors (1.3 for $volume\left(\frac{ZQC_{(P4-P2)}}{ZQC_{(P5-P2)}}\right)$, and 0.45 for $volume\left(\frac{ZQC_{(P6-P2)}}{ZQC_{(P5-P2)}}\right)$) are summarized in **Table 1**. All values are given in mean ± SD. Mean values were derived by performing six repeated measurements for each group (three measurements per mouse) within a day or two, while standard deviation was calculated as the square root of the variance. Saturation and unsaturation values were then calculated for each group using equation 1 and by using a fixed value of 2% for the level of triunsaturated fatty acids. By using equation 1 with the correction value of 1.3 ± 0.1 found experimentally, we found similar unsaturation levels for the two groups. However, when we compared the polyunsaturation level between the two groups, the difference between the standard diet and the PUFA diet group was quite dramatic. Using the 0.45 ± 0.08 experimental correction value and assuming a level of 2% of triunsaturated fatty acids and a negligible level of higher polyunsaturated fatty acids, we could calculate a diunsaturation level for the normal diet group of 18%, which is in pretty good agreement with what was found by Strobel et al. (16) for the diunsaturation level of NMRI mouse white adipose tissue (WAT). For the PUFA diet group, this calculation led to misleading results. In these mice, the presence of highly unsaturated (more than two double bonds) fatty acids led to a strong enhancement of the P6-P2 peak. Therefore, for this group, if we assumed a 2% level of triunsaturation, we arrived at an unreasonably high diunsaturation value, which after 12 weeks is larger than 100%.

This clearly indicates that for the PUFA group we cannot estimate the diunsaturation level because we cannot assume a value of only 2% of triunsaturation or neglect the presence of highly unsaturated fatty acids. For this group, we can only conclude that the comparison between the (P2-P4)/(P2-P5) ratio and the (P2-P6)/(P2-P5) shows a high level of highly unsaturated fatty acids that increased from week 4 to week 12 (**Fig. 4**).

DISCUSSION

We have demonstrated that 2D iZQC spectroscopy can provide an in vivo analysis of changes in adipose tissue composition related to diet intervention in mice. Signal from lean tissues is naturally suppressed by this method, and overall composition of small lipid depots that are scattered over large areas or that surround internal organs can be easily analyzed without the use of water suppression modules or small voxel selection.

Because this signal is only a small percentage of the standard proton signal, sensitivity can be a major limitation, especially in analyzing small volumes. However, when large tissues need to be analyzed, sensitivity can easily be improved by increasing the selected volume without incurring resolution degradation or signal contamination from nonfatty tissues.

By using this method, we can resolve saturated and unsaturated lipid components whose contribution, upon calibration, can be used to estimate the degree of unsaturation of overall fat composition in the body. The volumes corresponding to these peaks need to be corrected not only for transverse relaxation but also for RF pulse attenuation. Otherwise, the polyunsaturation level will be overestimated because a selective RF pulse is used in the protocol. This correction can be easily done before the procedure by collecting the 2D spectrum from a sample with a known value of the fraction of different fatty acids, as we have done here.

By using this method, we can detect the alterations in adipose lipid composition due to a PUFA-rich diet. Although such results cannot be directly compared with previous work, because of the different diet regiment, the alteration that we observed between the two groups are

TABLE 1. Peak ratios, FU, FD, and FM of mice fed a standard chow diet and mice fed with standard chow diet and PUFA supplements

Group	$volume\left(\frac{ZQC_{(P4-P2)}}{ZQC_{(P5-P2)}}\right)$	$volume\left(\frac{ZQC_{(P6-P2)}}{ZQC_{(P5-P2)}}\right)$	Unsaturation Level	FD	FM	FT Fixed
Standard diet (4 wks)						
Corrected	1.81 ± 0.15	0.22 ± 0.06	88.5 ± 7.5%	18 ± 6%	68.5 ± 10%	2%
Not corrected	1.39 ± 0.05	0.5 ± 0.1				
PUFA diet (4 wks)						
Corrected	1.69 ± 0.15	0.54 ± 0.1	84.5 ± 7.5%	50 ± 10%	30.5 ± 12%	2%
Not corrected	1.3 ± 0.05	1.2 ± 0.1				
Standard diet (12 wks)						
Corrected	1.68 ± 0.14	0.20 ± 0.06	83.5 ± 7%	16 ± 6%	63.5 ± 10%	2%
Not corrected	1.29 ± 0.05	0.45 ± 0.1				
PUFA diet (12 wks)						
Corrected	1.72 ± 0.15	1.22 ± 0.2	86 ± 7.5%	*118 ± 20%*	No calculation	2%
Not corrected	1.32 ± 0.05	2.7 ± 0.2				

All data are expressed as mean ± SD. The mean is calculated per group for a total of six measurements (three per mouse). The FT is fixed to a value of 2%, typical for rodent adipose tissue (16). Shown are the results corrected by using the experimental correction factors for the iZQC peaks. Diunsaturation and monounsaturation levels for high PUFA diet group are not reliable. For this group, the assumption that the fraction of triunsaturated fatty acids is only 2% or that highly unsaturated fatty acids are negligible does not hold. FD, fraction of diunsaturated fatty acids; FM fraction of monounsaturated fatty acids; FS, fraction of unsaturated fatty acids; FT fraction of triunsaturated fatty acids.

pretty consistent with the significant changes in adipose tissue composition found in previous studies on mice (27) and rats (28, 29), whose diet was supplemented with different oils or those found in adult humans on different diet regiments (11). As in those experiments, in the PUFA-rich diet, we observed a strong enhancement of the polyunsaturation level, which is reflected in a striking enhancement of the methylene-bisallylic iZQC peak with respect to the methylene-allylic peak. This enhancement, due to the presence of fatty acids with more than two double bonds, can be considered an amplification effect that can be used to track small changes in adipose tissue due to specific diet interventions.

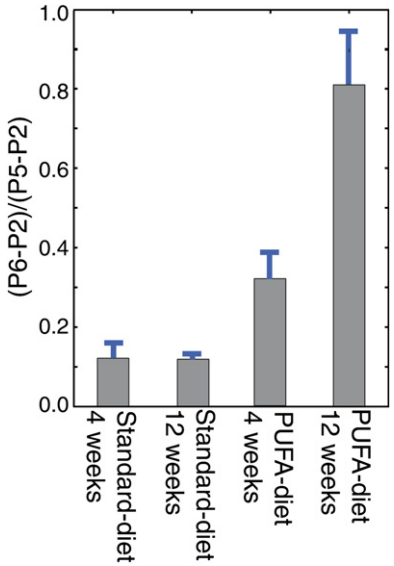

Fig. 4. Relative ratio between the bisallylic and the allylic iZQC peaks. The data are obtaining by calculating the ratio between the $volume\left(\frac{ZQC_{(P6-P2)}}{ZQC_{(P5-P2)}}\right)$ and the $volume\left(\frac{ZQC_{(P4-P2)}}{ZQC_{(P5-P2)}}\right)$ values reported in Table 1 from the two groups of animals. iZQC, intermolecular zero-quantum coherence spectroscopy.

In conclusion, our study indicates that the rapid acquisition of high-resolution NMR spectra of lipid depots scattered over different regions of the body is straightforward, and this method can provide information on lipid depots that are not accessible with standard NMR methods. The high resolution and sensitivity of the current method enables us to evaluate the impact of different diets on adipose tissue composition in situ, and it may also be used to study fatty acid composition of other highly heterogeneous organs, such as the liver. We anticipate that the method may be useful for the rapid detection of small changes in the composition of fatty acids in response to diet, exercise, and fat-metabolic diseases. In humans, such analyses could unveil differences due not only to different diets but also to lipid metabolism.

Despite the large spectral resolution improvements possible with this method, the possibility to separate the allylic protons from the α methylene protons at the more common lower clinical fields is conceivable but still need investigation. Although this method requires a specific modification of the standard spectroscopic sequences present on clinical scanners and is performed at relatively higher field with respect to standard clinical scanners, we strongly believe that this method will advance noninvasive human lipid research and aid the understanding of disorders that relate to disturbed lipid metabolism, including obesity, diabetes, and heart disease.

REFERENCES

1. Amri, E. Z., G. Ailhaud, and P. A. Grimaldi. 1994. Fatty acids as signal transducing molecules: involvement in the differentiation of preadipose to adipose cells. *J. Lipid Res.* **35:** 930–937.
2. Ntambi, J. M., and H. Bené. 2001. Polyunsaturated fatty acid regulation of gene expression. *J. Mol. Neurosci.* **16:** 273–278.
3. Clarke, S. D., D. Gasperikova, C. Nelson, A. Lapillonne, and W. C. Heird. 2002. Fatty acid regulation of gene expression. *Ann. N. Y. Acad. Sci.* **967:** 283–298.
4. Borkman, M., L. H. Storlien, D. A. Pan, A. B. Jenkins, D. J. Chisholm, and L. V. Campbell. 1993. The relation between insulin sensitivity and the fatty-acid composition of skeletal-muscle phospholipids. *N. Engl. J. Med.* **328:** 238–244.

5. Hotamisligil, G. S. 2006. Inflammation and metabolic disorders. *Nature.* **444:** 860–867.
6. Martin, D. D., M. E. Robbins, A. A. Spector, B. C. Wen, and D. H. Hussey. 1996. The fatty acid composition of human gliomas differs from that found in nonmalignant brain tissue. *Lipids.* **31:** 1283–1288.
7. Qiuhong, H. E., P. Shkarin, R. J. Hooley, D. R. Lannin, J. C. Weinreb, and V. I. J. Bossuyt. 2007. In vivo MR spectroscopic imaging of polyunsaturated fatty acids (PUFA) in healthy and cancerous breast tissues by selective multiple-quantum coherence transfer (Sel-MQC): a preliminary study. *Magn. Reson. Med.* **58:** 1079–1085.
8. Jucker, B. M., G. W. Cline, N. Barucci, and G. I. Shulman. 1999. Differential effects of safflower oil versus fish oil feeding on insulin-stimulated glycogen synthesis, glycolysis, and pyruvate dehydrogenase flux in skeletal muscle: a 13C nuclear magnetic resonance study. *Diabetes.* **48:** 134–140.
9. Winzell, M. S., G. Pacini, and B. Ahren. 2006. Insulin secretion after dietary supplementation with conjugated linoleic acids and n-3 polyunsaturated fatty acids in normal and insulin-resistant mice. *Am. J. Physiol. Endocrinol. Metab.* **290:** E347–E354.
10. Ikemoto, S., M. Takahashi, N. Tsunoda, K. Maruyama, H. Itakura, and O. Ezaki. 1996. High-fat diet-induced hyperglycemia and obesity in mice: differential effects of dietary oils. *Metabolism.* **45:** 1539–1546.
11. Hwang, J. H., S. Bluml, A. Leaf, and B. D. Ross. 2003. In vivo characterization of fatty acids in human adipose tissue using natural abundance 1H decoupled 13C MRS at 1.5 T: clinical applications to dietary therapy. *NMR Biomed.* **16:** 160–167.
12. Thomas, E. L., J. D. Hanrahan, M. Ala-Korpela, G. Jenkinson, D. Azzopardi, R. A. Iles, and J. D. Bell. 1997. Noninvasive characterization of neonatal adipose tissue by 13C magnetic resonance spectroscopy. *Lipids.* **32:** 645–651.
13. Fan, T. W., A. J. Clifford, and R. M. Higashi. 1994. In vivo 13C NMR analysis of acyl chain composition and organization of perirenal triacylglycerides in rats fed vegetable and fish oils. *J. Lipid Res.* **35:** 678–689.
14. Knothe, G., and J. A. Kenar. 2004. Determination of the fatty acid profile by 1H-NMR spectroscopy. *Eur. J. Lipid Sci. Technol.* **106:** 88–96.
15. Ren, J., I. Dimitrov, A. D. Sherry, and C. R. Malloy. 2008. Composition of adipose tissue and marrow fat in humans by 1H NMR at 7 Tesla. *J. Lipid Res.* **49:** 2055–2062.
16. Strobel, K., J. van den Hoff, and J. Pietzsch. 2008. Localized proton magnetic resonance spectroscopy of lipids in adipose tissue at high spatial resolution in mice in vivo. *J. Lipid Res.* **49:** 473–480.
17. Yeung, D. K., S. L. Lam, J. F. Griffith, A. B. Chan, Z. Chen, P. H. Tsang, and P. C. Leung. 2008. Analysis of bone marrow fatty acid composition using high-resolution proton NMR spectroscopy. *Chem. Phys. Lipids.* **151:** 103–109.
18. Ramamonjisoa, N., H. Ratiney, F. Rajas, E. Mutel, F. Pilleul, O. Beuf, and S. Cavassila. 2010. In vivo hepatic localized proton magnetic resonance spectroscopy at 7T in a glycogen storage disease mouse model. (Conference paper at ISMRM-ESMRMB Joint Annual Meeting. Stockholm, Sweden, May 1-7, 2010.
19. Van Werven, J. R., T. C. Schreuder, A. J. Nederveen, C. Lavini, P. L. Jansen, and J. Stoker. 2010. Hepatic unsaturated fatty acids in patients with non-alcoholic fatty liver disease assessed by 3.0T MR spectroscopy. *Eur. J. Radiol.* **75:** e102–e107.
20. Griffitts, J., Y. Tesiram, G. E. Reid, D. Saunders, R. A. Floyd, and R. A. Towner. 2009. In vivo MRS assessment of altered fatty acyl unsaturation in liver tumor formation of a TGF alpha/c-myc transgenic mouse model. *J. Lipid Res.* **50:** 611–622.
21. Ruberg, F. L., J. Viereck, A. Phinikaridou, Y. Qiao, J. Loscalzo, and J. A. Hamilton. 2006. Identification of cholesteryl esters in human carotid atherosclerosis by ex vivo image-guided proton MRS. *J. Lipid Res.* **47:** 310–317.
22. Vathyam, S., S. Lee, and W. S. Warren. 1996. Homogeneous NMR spectra in inhomogeneous fields. *Science.* **272:** 92–96.
23. Lin, Y., S. Ahn, N. Murali, W. Brey, C. R. Bowers, and W. S. Warren. 2000. High-resolution, >1 GHz NMR in unstable magnetic fields. *Phys. Rev. Lett.* **85:** 3732–3735.
24. Faber, C., E. Pracht, and A. Haase. 2003. Resolution enhancement in vivo NMR spectroscopy: detection of intermolecular zero-quantum coherences. *J. Magn. Reson.* **161:** 265–274.
25. Balla, D. Z., and C. Faber. 2007. In vivo intermolecular zero-quantum coherence MR spectroscopy in the rat spinal cord at 17.6 T: a feasibility study. *Magn. Reson. Mater. Phys. Biol. Med. (Paris).* **20:** 183–191.
26. Balla, D. Z., G. Melkus, and C. Faber. 2006. Spatially localized intermolecular zero-quantum coherence spectroscopy for in vivo applications. *Magn. Reson. Med.* **56:** 745–753.
27. Tove, S. B., and F. Smith. 1960. Changes in the fatty acid composition of the depot fat of mice induced by feeding oleate and linoleate. *J. Nutr.* **71:** 264–272.
28. Awad, A. B. 1981. Effect of dietary lipids on composition and glucose utilization by rat adipose tissue. *J. Nutr.* **111:** 34–39.
29. Valero-Garrido, D., M. Lopez-Frias, J. Llopis, and M. Lopez-Jurado. 1990. Influence of dietary fat on the lipid composition of perirenal adipose tissue in rats. *Ann. Nutr. Metab.* **34:** 327–332.